Penny-shaped cracks by Finite Fracture Mechanics

PENNY-SHAPED CRACKS BY FINITE FRACTURE MECHANICS

P. Cornetti (*), A. Sapora

Department of Structural, Building and Geotechnical Engineering
Politecnico di Torino, Corso Duca degli Abruzzi 24, 10129, Torino, Italy.

Abstract

In this brief note, we provide the failure stress of a solid containing a penny-shaped crack by means of Finite Fracture Mechanics. The solution is analytical up to the numerical root of the equation providing the finite crack growth increment. Results are discussed and compared with the ones provided by Linear Elastic Fracture Mechanics, by Theory of Critical Distances and by Cohesive Crack Model (with a Dugdale-type cohesive law).

Keywords: Finite Fracture Mechanics, Cohesive Crack Model, Penny-Shaped Crack.

1. Introduction

Finite Fracture Mechanics (FFM) is a fracture criterion resting on the assumption of a discrete crack growth; as such, it differs from Linear Elastic Fracture Mechanics (LEFM) where crack propagation is assumed to be continuous. Failure load predictions are achieved by means of the discrete energy balance (which substitutes the infinitesimal Griffith one exploited by LEFM) coupled with a suitable stress condition. While LEFM works for cracked structures only, FFM is able to provide sound strength predictions for cracked, notched or plain structures. FFM works for quasi-brittle materials and is a two-material parameter model, requiring the tensile strength and fracture energy (or toughness) for use.

Several models considering crack jumps or a discontinuous crack growth had been proposed in the past (e.g. Kfouri, 1979; Neimitz & Aifantis, 1987; Hashin, 1996; Pugno & Ruoff, 2004). Leguillon first set the FFM approach in 2002 (Leguillon, 2002). Since that, several successful applications of FFM have been provided and nowadays FFM can be regarded as an effective tool to predict the strength of mechanical components (e.g. Cornetti et al., 2006; Yosibash et al., 2006; Mantič, 2009; Camanho et al., 2012; Weißgraeber & Becker, 2013; Felger et al., 2019), allowing fast strength predictions suitable for preliminary sizing of structures.

(*) corresponding author. Email: pietro.cornetti@polito.it; tel.: +390110904901; fax: +390110904899

Most of FFM applications deal with 2D geometries. Only recently, some attempts have been done to extend the fracture criterion to 3D cases (Leguillon, 2014; Yosibash & Mittelman, 2016; García et al. 2016; Doitrand & Leguillon, 2018). The 3D case is of course much more complex for several reasons, e.g. the change of the crack shape as crack grows. In the present paper we will analyze the case of a (infinite) body containing a penny-shaped crack subjected to a remote uniform stress orthogonal to the crack, which is actually the simplest 3D geometry one can consider. In fact, although the problem is three-dimensional, the axial symmetry (the crack remains circular during its growth) makes the FFM analysis relatively simple, yet interesting for the geometry itself and for possible future 3D extensions. In this respect, the present investigation is analogous to the spherical particle debonding problem analyzed by Gentieu et al. (2019).

The paper is organized as follows. After the Introduction, Section 2 briefly recalls the stress and displacement field for a penny-shaped crack. In Section 3, we apply FFM to get the failure stress estimate. In Section 4, since the geometry analyzed is hard to reproduce experimentally, we validate the FFM approach by comparison with the widely used Cohesive Crack Model (CCM) and the Theory of Critical Distances (TCD). Conclusions are finally given in Section 5.

2. The penny-shaped crack

Let us consider an infinite body containing a crack having the shape of a disk of radius a. The cylindrical coordinate system has the origin at the center of the crack and the reference plane is the one containing the crack. The radial coordinate is r and the axial coordinate is z. The third coordinate is the azimuth φ but it will not be used because of axial symmetry. The body is loaded by a uniform remote stress σ_∞ at infinity in the z direction, so that the crack is in Mode I opening conditions (see Fig. 1).

The solution for such a geometry within the linear elasticity theory dates back to Sneddon (1946); see also Bertram Broberg (1999). Accordingly, the longitudinal stresses in the reference (crack) plane ($z = 0$) are given by:

$$\sigma_z(r) = \frac{2}{\pi}\sigma_\infty\left[\frac{a}{\sqrt{r^2-a^2}} + \arccos\frac{a}{r}\right], \qquad r > a \quad (1)$$

It follows that the Stress Intensification Factor (SIF) is equal to:

$$K_I = \lim_{r \to a^+} \sigma_z \sqrt{2\pi(r-a)} = 2\sigma_\infty \sqrt{\frac{a}{\pi}} \qquad (2)$$

The longitudinal displacement on the upper crack face ($z = 0^+$) is:

$$u_z(r) = \frac{4(1-\nu^2)}{\pi E} \sigma_\infty \sqrt{a^2 - r^2}, \qquad r \le a \quad (3)$$

which is half of the crack opening displacement. E and ν are the Young's modulus and the Poisson's coefficient of the material, respectively. Eqs. (1-3) are enough to apply FFM. However, in order to compare FFM with CCM in Section 4, we need also some results for the case of a penny-shaped crack where the (crack) annular surface $b < r < a$ (and $z = 0$) is loaded by a uniform (opening) stress p (see Fig. 2). Accordingly, the SIF is (Tada et al., 2000):

$$K_I = \frac{2p}{\sqrt{\pi a}} \sqrt{a^2 - b^2} \qquad (4)$$

which reverts to Eq. (2) as $b \to 0$. Finally, the longitudinal displacement at the border of the loaded and un-loaded region of the upper crack surface ($z = 0^+$) is:

$$u_z(r = b) = \frac{4(1-\nu^2)}{\pi E} p\,(a - b) \qquad (5)$$

3. Finite Fracture Mechanics

According to the FFM approach, a necessary condition for a finite crack to occur is that the energy available for the crack growth must be higher than the energy required to create the new fracture surface. Thus, we need to evaluate the strain energy increment $\Delta\phi$ passing from the original geometry to the final one, i.e. after the finite crack extension. Because of axial symmetry, we can assume the crack increment to be annular from $r = a$ up to $r = a + \Delta$. The strain energy increment equals the crack closure work, so that we can get $\Delta\phi$ as half of the product of the stress before crack advance (Eq. (1))

and the displacement after crack advance (Eq. (3) with a replaced by $a + \Delta$) integrated over the new crack surface:

$$\Delta\phi = \frac{1}{2}\int_{a}^{a+\Delta} 2\,u_z(a+\Delta, r)\,\sigma_z(a, r)\,2\pi r\,\mathrm{d}r \quad (6)$$

where $2u_z$ is the crack opening. Hence, by means of Eqs. (1) and (3):

$$\Delta\phi = \frac{16(1-\nu^2)}{\pi E}\sigma_\infty^2 \int_{a}^{a+\Delta} \sqrt{(a+\Delta)^2 - r^2}\left[\frac{a}{\sqrt{r^2-a^2}} + \arccos\frac{a}{r}\right] r\,\mathrm{d}r \quad (7)$$

The integration yields:

$$\Delta\phi = \frac{8\,(1-\nu^2)}{3\,E}\,\sigma_\infty^2\,\Delta\left(3a^2 + 3a\Delta + \Delta^2\right) \quad (8)$$

The same result can be obtained by means of Irwin's relationship and the SIF (Eq. (2)):

$$\Delta\phi = \int_{a}^{a+\Delta} \mathcal{G}(a')\,2\pi a'\mathrm{d}a' = \frac{(1-\nu^2)}{E}\int_{a}^{a+\Delta} K_{\mathrm{I}}^2(a')\,2\pi a'\mathrm{d}a' = \frac{8(1-\nu^2)}{E}\sigma_\infty^2\int_{a}^{a+\Delta}(a')^2\,\mathrm{d}a' \quad (9)$$

which, upon integration, confirms Eq. (8). For the crack to propagate, the strain energy increment must be higher than the energy necessary to create the new (annular) crack surface. Introducing the material fracture energy $\mathcal{G}_c$, this implies that:

$$\frac{8\,(1-\nu^2)}{3\,E}\,\sigma_\infty^2\,\Delta\left(3a^2 + 3a\Delta + \Delta^2\right) \geq \mathcal{G}_c\pi\left[(a+\Delta)^2 - a^2\right] \quad (10)$$

Irwin's relationship and length l_{ch} are, respectively:

$$K_{\mathrm{Ic}} = \sqrt{\frac{\mathcal{G}_c E}{(1-\nu^2)}}, \qquad l_{\mathrm{ch}} = \left(\frac{K_{\mathrm{Ic}}}{\sigma_c}\right)^2 \quad (11)$$

where K_{Ic} is the material fracture toughness and σ_c the material tensile strength. Accordingly, Eq. (10) yields:

$$\frac{\sigma_\infty}{\sigma_c} \geq \sqrt{\frac{3}{8}\pi l_{ch}\,\frac{2a+\Delta}{3a^2+3a\Delta+\Delta^2}} \qquad (12)$$

Eq. (12) shows that, for a given crack size and according to the discrete energy balance, the remote stress causing crack propagation decreases as the crack increment increases (see Fig.3).

The latter condition for crack growth is a stress requirement. According to Leguillon's FFM approach, we can require that, before the crack increment, the stress exceeds the material tensile strength on the region where the crack step will take place, i.e. $\sigma_z(r) \geq \sigma_c$ for $a \leq r \leq (a+\Delta)$. Since the stress field ahead the crack tip is monotonically decreasing, this condition is tantamount requiring that:

$$\sigma_z\left(r = a+\Delta\right) \geq \sigma_c \qquad (13)$$

By using the stress field Eq. (1), one gets:

$$\frac{\sigma_\infty}{\sigma_c} \geq \frac{\pi}{2}\frac{\sqrt{\Delta(2a+\Delta)}}{a+\sqrt{\Delta(2a+\Delta)}\,\arccos\dfrac{a}{a+\Delta}} \qquad (14)$$

Eq. (14) shows that, for a given crack size and according to the stress condition (13), the remote stress causing crack propagation increases as the crack increment increases (see Fig. 3).

According to FFM, both conditions (12) and (14) are necessary for crack growth. If contemporaneously fulfilled, they become also a sufficient condition. Of course, the actual failure stress is the minimum for which both the inequalities are satisfied. Because of the monotonic behavior of the conditions, the minimum remote failure stress is achieved when both the conditions are strictly fulfilled (Fig. 3). It means that the actual crack advance is given by the root Δ_c of the equation obtained by equating the right hand sides of Eqs. (12) and (14), i.e.:

$$2\pi\Delta(3a^2+3a\Delta+\Delta^2) = 3l_{ch}\left[a+\sqrt{\Delta(2a+\Delta)}\,\arccos\frac{a}{a+\Delta}\right]^2 \qquad (15)$$

The remote failure stress σ_f is finally achieved upon substitution of the root of Eq. (15) into either the right hand side of Eq. (12) or Eq. (14). Results are plotted in Figs.4 and 5. As the crack size increases, the finite crack extension decreases from $(3/8 \cdot \pi) \times l_{ch}$ to $(1/2\pi) \times l_{ch}$, while the failure stress drops from the tensile strength to zero. The failure stress vs. crack radius is plotted also in bi-logarithmic scale in Fig. 6, which shows the typical LEFM 1/2 slope for large sizes.

4. Comparison with existing models and similar geometries

4.1 LEFM

We start comparing the result by the FFM approach with LEFM predictions (i.e. $K_I = K_{Ic}$), which, in dimensionless form, reads:

$$\frac{\sigma_f}{\sigma_c} = \frac{1}{2}\sqrt{\pi \frac{l_{ch}}{a}} \qquad (16)$$

As expected (see Figs.5-6), FFM and LEFM predictions tend to merge for large crack size: relative differences are lower than 1% for crack radii larger than about $4 \times l_{ch}$. For smaller cracks, it is evident that LEFM provides higher (and thus potentially dangerous) predictions with respect to FFM, becoming furthermore unreliable when $a < (\pi/4) \times l_{ch}$ since Eq. (16) yields failure stresses higher than the tensile strength. Hence, according to LEFM, structures are insensitive to penny-shaped defects with radius lower than $(\pi/4) \times l_{ch}$. On the other hand, FFM predictions are affected by penny-shaped crack of any size, although the failure stress vs. crack radius curve shows a flat tangent in the origin and an almost constant value (difference below 1%) for crack radii below about $(\pi/8) \times l_{ch}$.

4.2 Theory of critical distances

Theory of Critical Distances (TCD) are a set of stress failure criteria that, beyond the strength, take also the fracture toughness into account by means of a suitable characteristic distance (Taylor, 2007). In such a way, TCD extends the applicability of stress failure criteria to structures where stress singularities or high stress gradients occur. Among TCD approaches, the simplest and most used one is the Point Method (PM). According to PM, failure is achieved when the stress at a distance $(1/2\pi) \times l_{ch}$ ahead the crack tip (or the stress concentration point) reaches the tensile strength. In the geometry at hand, this means, by Eq. (1):

$$\frac{\sigma_f}{\sigma_c} = \frac{\pi}{2} \frac{\sqrt{l_{ch}(4\pi a + l_{ch})}}{2\pi a + \sqrt{l_{ch}(4\pi a + l_{ch})}\,\arccos\left(\frac{2\pi a}{2\pi a + l_{ch}}\right)} \quad (17)$$

Although able to predict the transition between the strength-governed failure for a vanishing crack and the energy-driven failure for large crack sizes, Figs. 4 and 5 show that PM predictions are significantly lower with respect to the FFM ones (up to 16%). Considering the FFM approach as more accurate, we may say that PM provides too conservative predictions.

4.3 Cohesive Crack Model

For the penny-shaped crack, it is also possible to achieve analytical solution by means of a Dugdale-type CCM, i.e. with a rectangular cohesive law, see Fig. 7. According to Dugdale (1960) model, a plastic annular region of radial size a_p appears ahead the crack tip where stresses are constant and equal to σ_c. The size of this zone is determined by imposing that the SIF at $r = a + a_p$, i.e. at the *fictitious* crack tip, is null. By Eqs. (2) and (4), one gets:

$$K_I = 2\sigma_\infty \sqrt{\frac{a + a_p}{\pi}} - \frac{2\sigma_c}{\sqrt{\pi(a + a_p)}} \sqrt{(a + a_p)^2 - a^2} = 0 \qquad (18)$$

Hence (see, e.g. Kelly & Nowell, 2000):

$$\frac{a_p}{a} = \frac{1}{\sqrt{1 - (\sigma_\infty / \sigma_c)^2}} - 1 \qquad (19)$$

meaning that the plastic (or process) zone size is zero when the remote stress is zero and infinite when the remote stress approaches the tensile strength. Crack growth will occur when the opening displacement at the *real* (i.e. at $r = a$) crack tip reaches the critical value $w_c = \mathcal{G}_c/\sigma_c$ (see Fig. 7). By Eqs. (3) and (5), one gets:

$$\frac{8(1 - \nu^2)}{\pi E} \left[\sigma_\infty \sqrt{(a + a_p)^2 - a^2} - \sigma_c a_p \right] = w_c \qquad (20)$$

By inserting Eq. (19) into (20), we finally get the failure stress and the related process zone size vs. the crack radius a as:

$$\frac{\sigma_f}{\sigma_c} = \sqrt{1-\left(1-\frac{\pi}{8}\frac{l_{ch}}{a}\right)^2} \qquad (21)$$

$$a_p = \frac{\frac{\pi}{8}l_{ch}}{1-\frac{\pi}{8}\frac{l_{ch}}{a}} \qquad (22)$$

Obviously Eqs. (21) and (22) hold for crack radii larger than $(\pi/8)\times l_{ch}$. Below, a_p is infinite and the failure stress equals the tensile stress. Results are plotted in Figs. 4 to 6. For what concerns the process zone (Fig. 4), it shows a monotonically decreasing trend with respect to the crack radius as the finite crack extension does. Furthermore, $a_p \to (\pi/8)\times l_{ch}$ as $a \to \infty$, i.e. a_p tends to the classical Dugdale plastic zone estimate for large cracks, as expected. For what concerns the failure stress (Fig. 5), the agreement between FFM and CCM is excellent: relative differences remain always below 4%. This result validates the present FFM approach.

4.4 Average stress Finite Fracture Mechanics

One can also couple the discrete energy balance Eq. (10) through an average stress condition (Cornetti et al., 2006), i.e. requiring the *average* normal stress before crack advance to exceed the tensile strength. This means replacing Eq. (13) with the following equation:

$$\int_a^{a+\Delta} \sigma_z 2\pi r \, dr \geq \sigma_c \pi\left[(a+\Delta)^2 - a^2\right] \qquad (23)$$

Upon substitution of Eq. (1), Eq. (23) yields:

$$\frac{\sigma_\infty}{\sigma_c} \geq \frac{\pi}{2}\frac{\Delta(2a+\Delta)}{a\sqrt{\Delta(2a+\Delta)} + (a+\Delta)^2 \arccos\frac{a}{a+\Delta}} \qquad (24)$$

Eq. (24) coupled with Eq. (12) provides the finite crack extension, decreasing from $(3/8 \cdot \pi) \times l_{ch}$ to $(2/\pi) \times l_{ch}$ as the crack radius increases (see Fig. 4), and the corresponding failure stress, which is compared with Leguillon's FFM in Fig. 8. It is evident that Cornetti's FFM provides lower estimate

for the failure stress. This is a general feature; moreover, average stress FFM is usually in agreement with CCM characterized by a linear softening cohesive law (Cornetti et al., 2019).

4.5 Griffith crack

In Fig. 9 we compare the FFM (and LEFM) failure stress estimates for a penny-shaped crack with the ones for a Griffith crack, i.e. a through-thickness crack in an infinite plate subjected to a remote uniform uniaxial stress orthogonal to the crack. The half-length of the Griffith crack is a and it is assumed to be equal to the radius of the penny-shaped crack. The FFM solution for the Griffith crack is given in Cornetti et al. (2014, 2016). The comparison is interesting because it shows that the knee point defining the transition between the small crack stress-governed failure and the large crack energy-driven rupture occurs for the penny-shaped crack at a higher a value (about $(\pi/4) \times l_{ch}$ instead of $(1/\pi) \times l_{ch}$ holding for the Griffith crack) as clearly evidenced in Fig. 9. Relative differences lower than 1% between FFM and the corresponding LEFM solutions occurs anyway at about the same value ($4 \times l_{ch}$).

5. Conclusions

In the present paper, we provided the FFM solution for a penny-shaped crack under mode I conditions and remote uniform normal stresses. Classical Fracture Mechanics results allowed us to achieve the solution in a semi-analytical form. The problem is three-dimensional, leading to some differences with respect to the two-dimensional FFM applications already available in the Scientific Literature. The model was finally validated by comparing the FFM solution with the CCM approach. The excellent agreement corroborates the use of FFM as an effective tool to assess the safety of structural components.

Figure captions

Figure 1. Penny-shaped crack under uniform remote stress: 3D view (a); longitudinal section (b).

Figure 2. Penny-shaped crack under annular constant stresses: 3D view (a); longitudinal section (b).

Figure 3. Admissible failure stresses vs. finite crack increment according to discrete energy balance and stress requirement for $a = 0.6\ l_{ch}$. The actual failure stress is the minimum among admissible values.

Figure 4. Finite crack increment according to FFM approaches and process zone size at incipient failure according to CCM vs. crack radius.

Figure 5. Failure stress according to FFM, LEFM, PM and CCM vs. crack radius.

Figure 6. Failure stress according to FFM, LEFM, PM and CCM vs. crack radius (bi-logarithmic plot).

Figure 7. Dugdale-type cohesive law.

Figure 8. Failure stress vs. crack radius according to FFM coupled with point-wise and average stress conditions.

Figure 9. Failure stress for a solid containing a penny-shaped crack (continuous line) and for a slab containing a through-thickness crack (dashed line) vs. crack radius/half-length according to FFM and LEFM.

References

Bertram Broberg K. (1999) *Cracks and fracture*. Academic Press. London.

Camanho P.P., Erçin G.H., Catalanotti G., Mahdi S., Linde P. (2012). *A finite fracture mechanics model for the prediction of the open-hole strength of composite laminates*. Composites: Part A 43:1219-1225.

Cornetti P., Muñoz-Reja M., Sapora A., Carpinteri A. (2019) *Finite fracture mechanics and cohesive crack model: Weight functions vs. cohesive laws*. International Journal of Solids and Structures 156-157: 126-136.

Cornetti P., Pugno N., Carpinteri A., Taylor D. (2006) *Finite fracture mechanics: a coupled stress and energy failure criterion*. Engineering Fracture Mechanics 73:2021-2033.

Cornetti P., Sapora A., Carpinteri A. (2014) *Finite fracture mechanics vs. Cohesive crack modelling: An analytical comparison based on case studies*. 16th European Conference on Composite Materials, ECCM 2014.

Cornetti P., Sapora A., Carpinteri A. (2016) *Short cracks and V-notches: Finite Fracture Mechanics vs. Cohesive Crack Model*. Engineering Fracture Mechanics 168:2-12.

Doitrand A., Leguillon D. (2018) *3D application of the coupled criterion to crack initiation prediction in epoxy/aluminum specimens under four point bending*. International Journal of Solids and Structures 143:175-182.

Dugdale D.S. (1960) *Yielding of steel sheets containing slits*. Journal of the Mechanics and Physics of Solids 8:100-108.

Felger J., Rosendahl P.L., Leguillon D., Becker W. (2019) *Predicting crack patterns at bi-material junctions: A coupled stress and energy approach*. International Journal of Solids and Structures. In press.

García I.G., Carter B.J., Ingraffea A.R., Mantič V. (2016) *A numerical study of transverse cracking in cross-ply laminates by 3D finite fracture mechanics*. Composites Part B 95:475-487.

Gentieu T., Jumel J., Catapano A., Broughton J. (2019). *Size effect in particle debonding: Comparisons between finite fracture mechanics and cohesive zone model*. Journal of Composite Materials (in press)

Hashin Z. (1996) *Finite thermoelastic fracture criterion with application to laminate cracking analysis*. Journal of the Mechanics and Physics of Solids 44:1129-1145.

Kelly P.A., Nowell D. (2000) *Three-dimensional cracks with Dugdale-type plastic zones*. International Journal of Fracture 106:291-309.

Kfouri A.P. (1979) *Continuous crack growth or quantized growth steps?* International Journal of Fracture, 15:23-29.

Leguillon D. (2002) *Strength or toughness? A criterion for crack onset at a notch*. European Journal of Mechanics A/Solids 21:61-72.

Leguillon D. (2014) *An attempt to extend the 2D coupled criterion for crack nucleation in brittle materials to the 3D case*. Theoretical and Applied Fracture Mechanics 74:7-17.

Mantič V. (2009) *Interface crack onset at a circular cylindrical inclusion under a remote transverse tension. Application of a coupled stress and energy criterion*. International Journal of Solids and Structures 46:1287-1304.

Neimitz A., Aifantis E.C. (1987) *On the length of crack jump during subcritical growth*. Engineering Fracture Mechanics 26:505-518.

Pugno N.M., Ruoff R.S. (2004) *Quantized fracture mechanics*. Philosophical Magazine 84:2829-2845.

Sapora A., Cornetti P. (2018) *Crack onset and propagation stability from a circular hole under biaxial loading*. International Journal of Fracture 214:97-104

Sneddon I.N. (1946) *The distribution of stress in the neighbourhood of a crack in an elastic solid*. Proceedings of the Royal Society (London) A187:229-260

Tada H., Paris P., Irwin G. (2000) *The Stress Analysis of Cracks Handbook*. ASME Press. New York.

Taylor D. (2007) *The Theory of Critical Distances*. Elsevier Science.

Weißgraeber P., Becker W. (2013) *Finite Fracture Mechanics model for mixed mode fracture in adhesive joints*. International Journal of Solids and Structures 50:2383-2394.

Yosibash Z., Mittelman B. (2016). A 3-D failure initiation criterion from a sharp V-notch edge in elastic brittle structures. European Journal of Mechanics - A/Solids, 60:70-94.

Yosibash Z., Priel E., Leguillon D. (2006) *A failure criterion for brittle elastic materials under mixed-mode loading*. International Journal of Fracture 141:291-312.

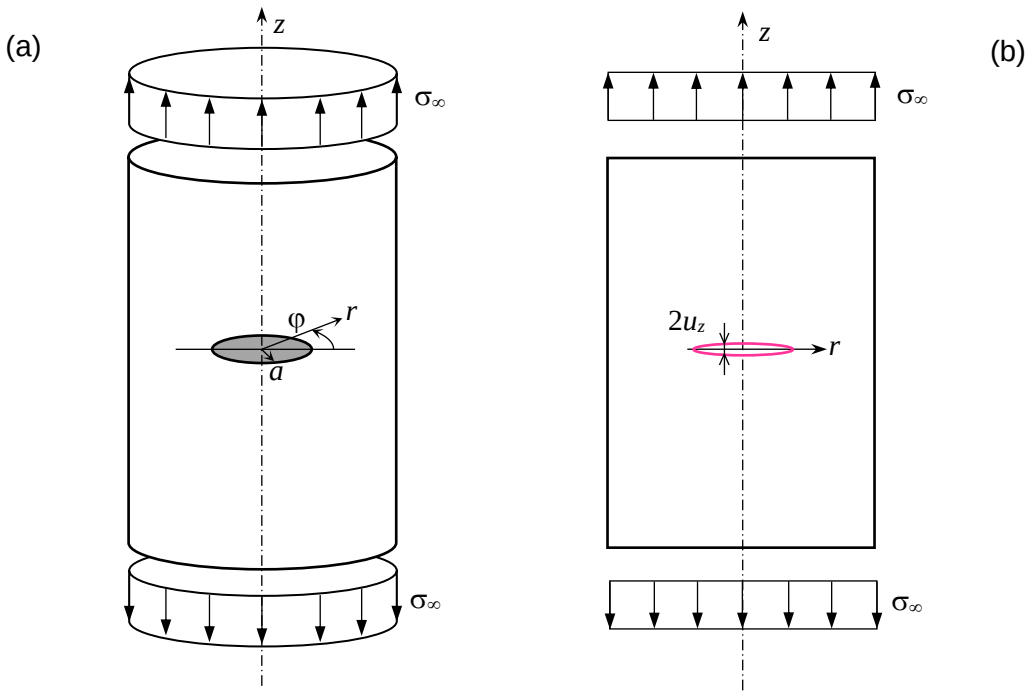

Figure 1. Penny-shaped crack under uniform remote stress: 3D view (a); longitudinal section (b).

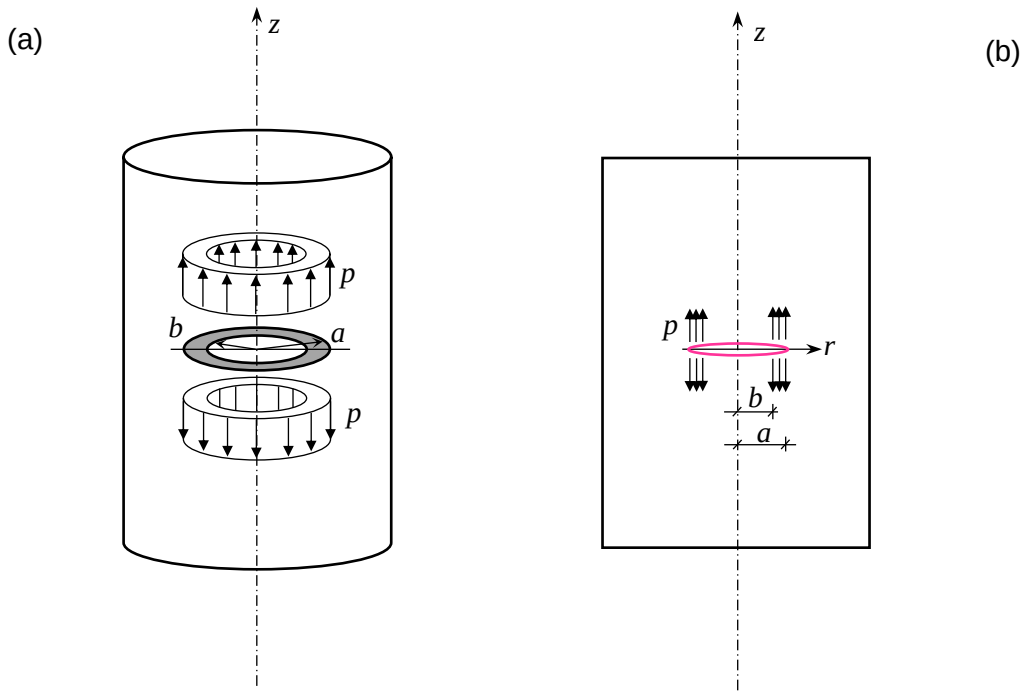

Figure 2. Penny-shaped crack under annular constant stresses: 3D view (a); longitudinal section (b).

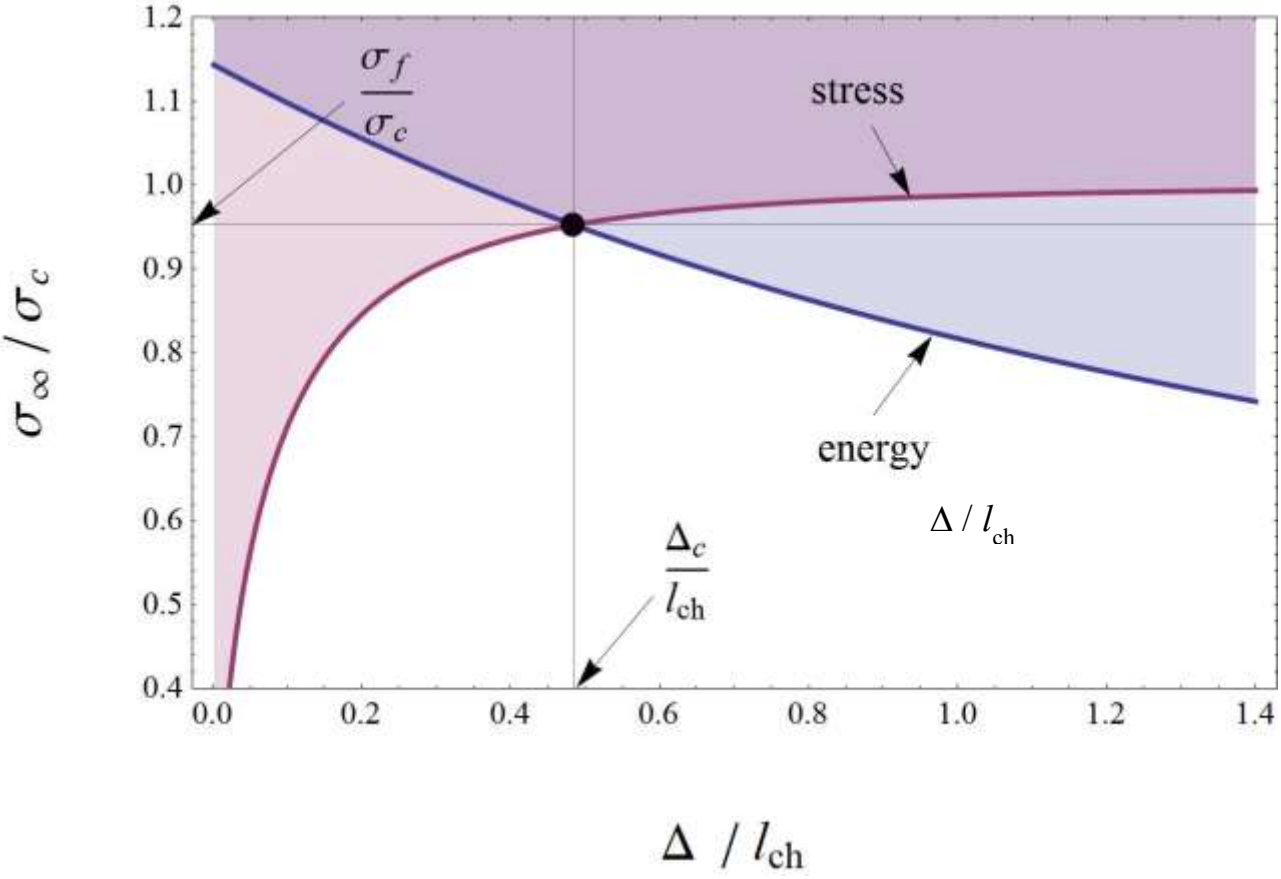

Figure 3. Admissible failure stresses vs. finite crack increment according to discrete energy balance and stress requirement for $a = 0.6\, l_{ch}$. The actual failure stress is the minimum among admissible values.

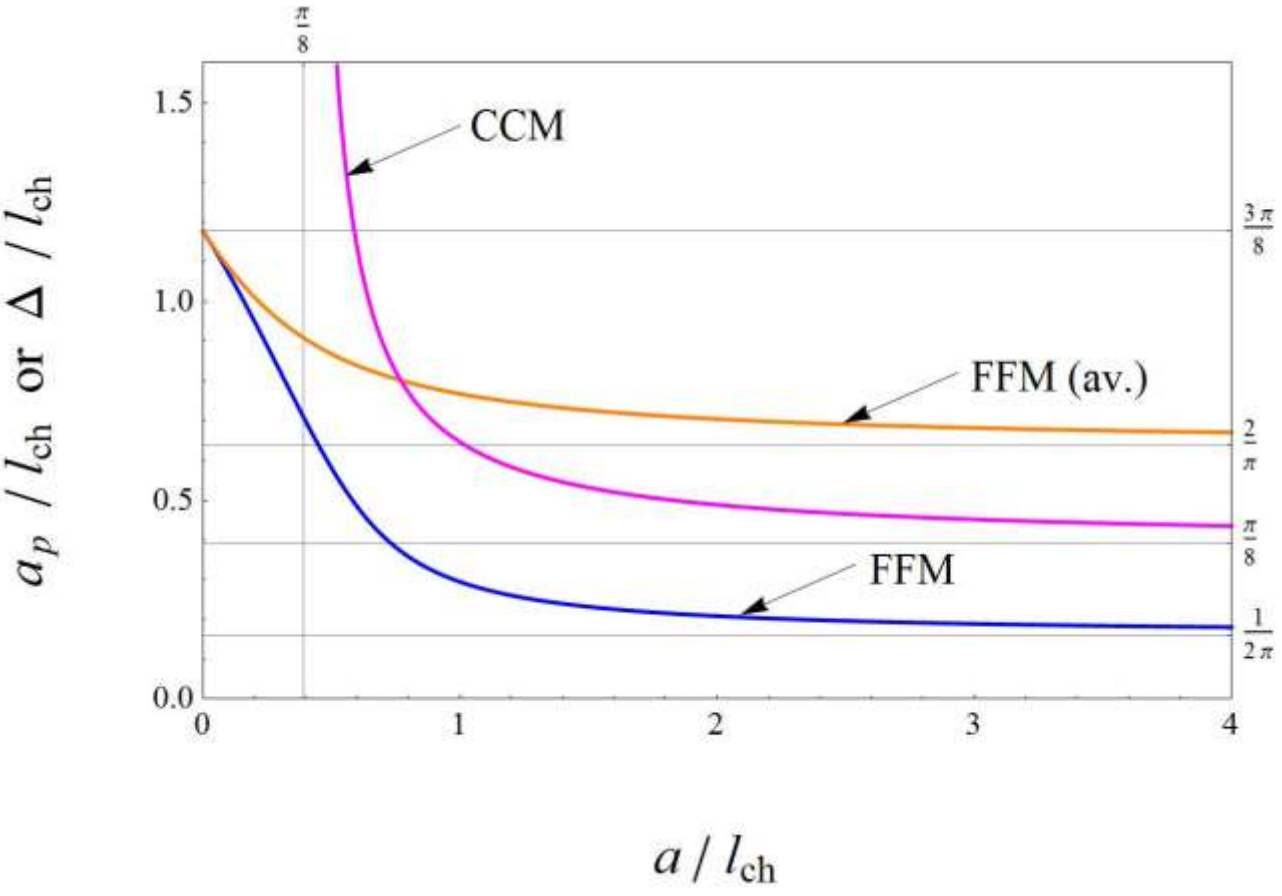

Figure 4. Finite crack increment according to FFM approaches and process zone size at incipient failure according to CCM vs. crack radius.

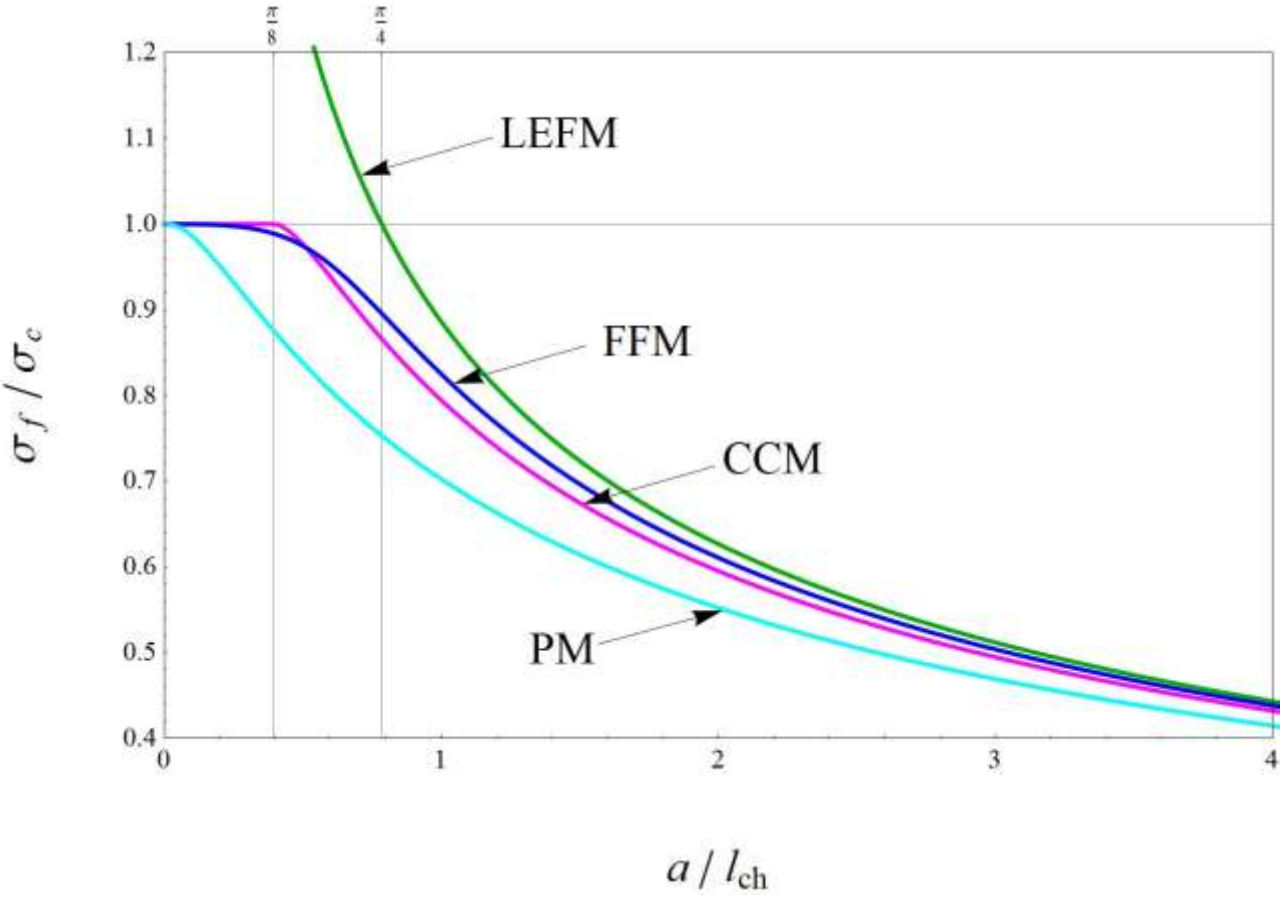

Figure 5. Failure stress according to FFM, LEFM, PM and CCM vs. crack radius.

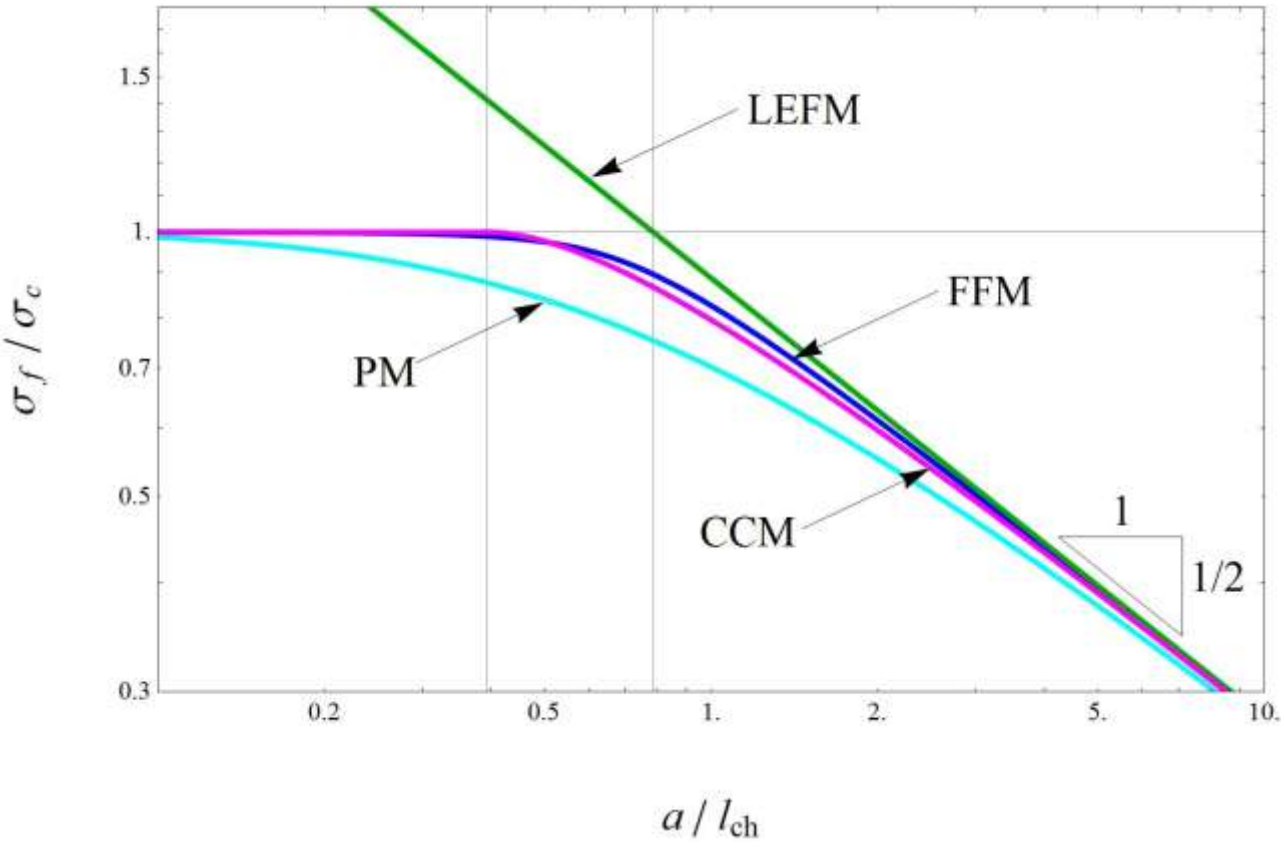

Figure 6. Failure stress according to FFM, LEFM, PM and CCM vs. crack radius (bi-logarithmic plot).

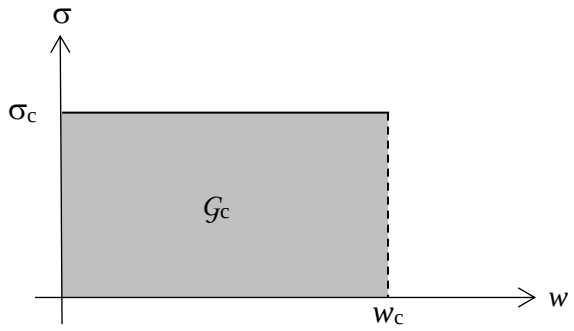

Figure 7. Dugdale-type cohesive law.

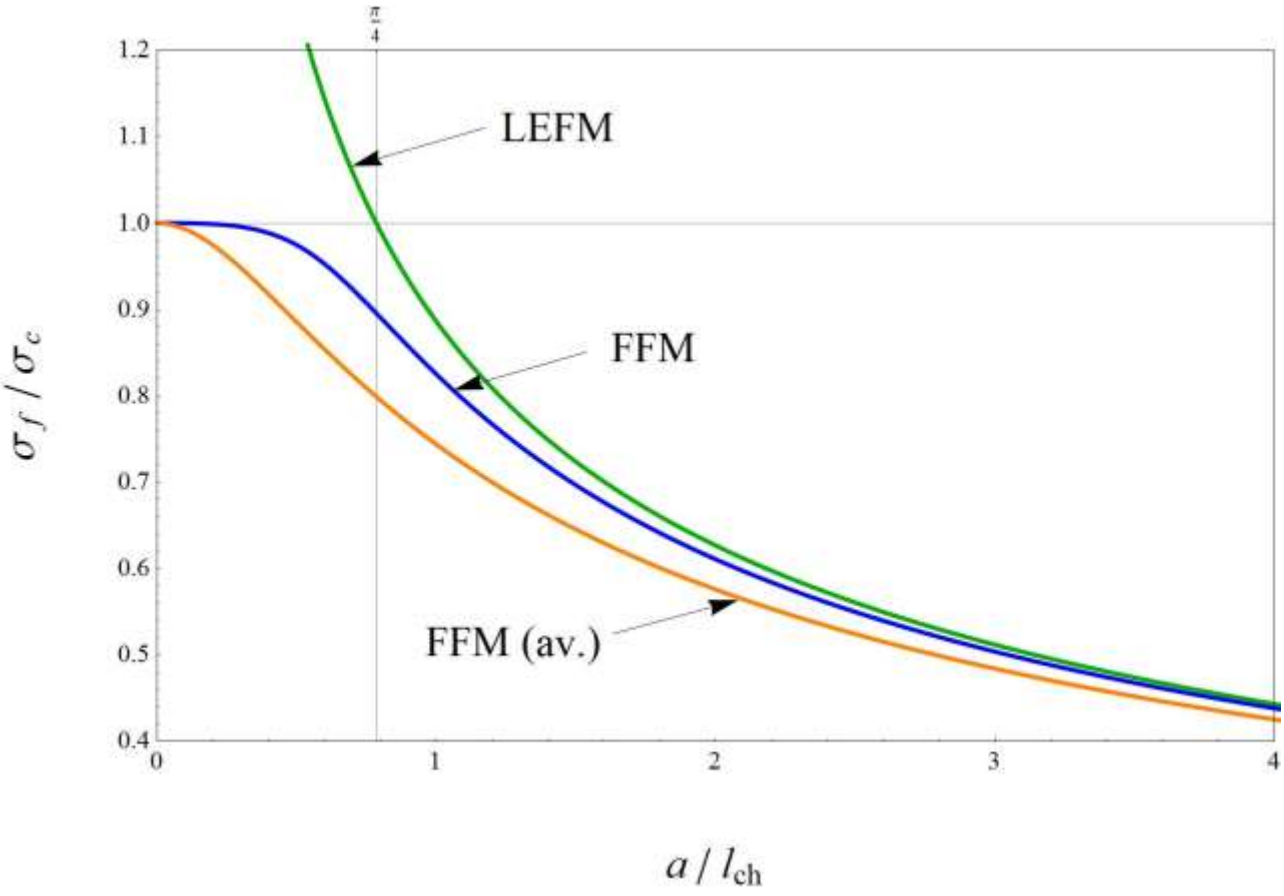

Figure 8. Failure stress vs. crack radius according to FFM coupled with point-wise and average stress conditions.

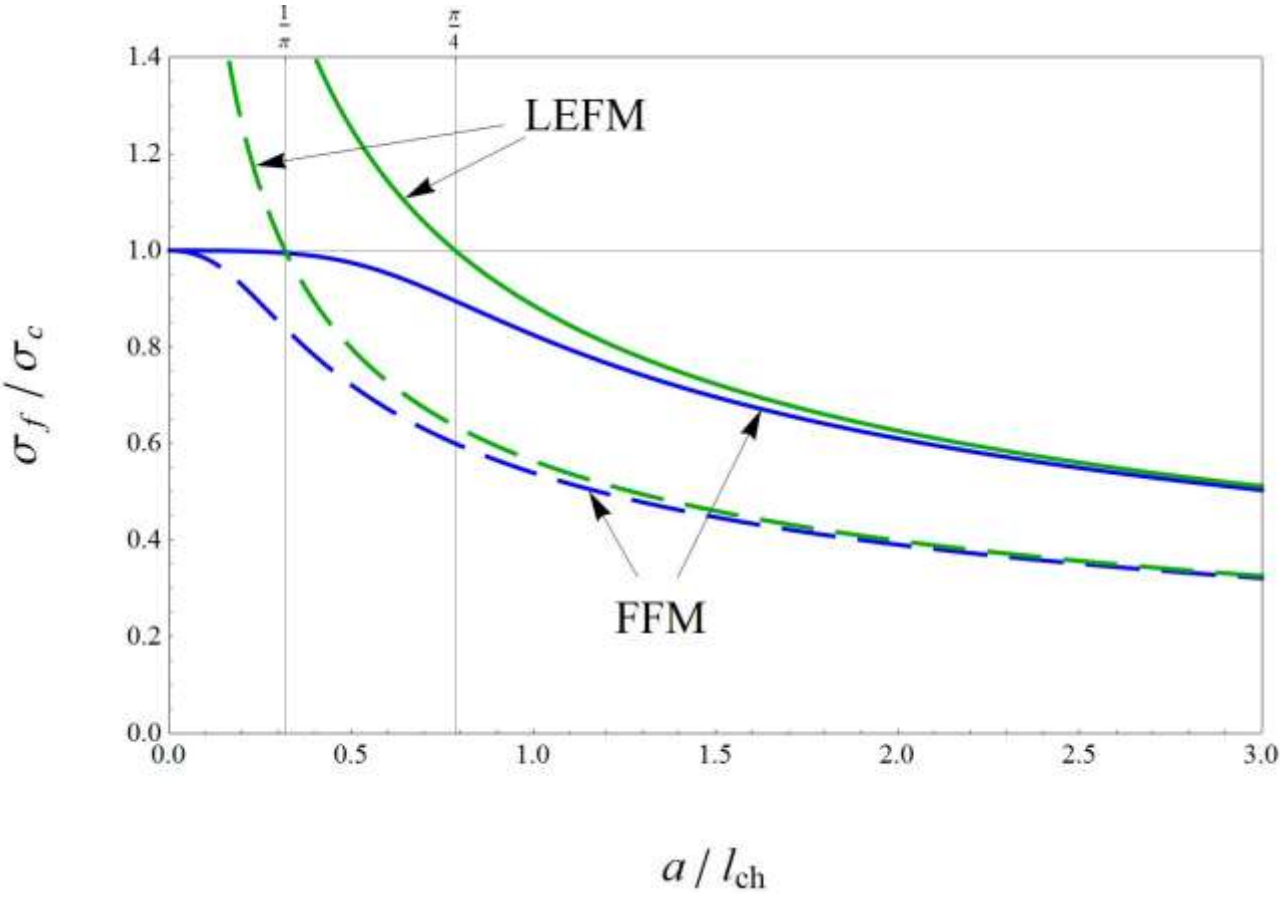

Figure 9. Failure stress for a solid containing a penny-shaped crack (continuous line) and for a slab containing a through-thickness crack (dashed line) vs. crack radius/half-length according to FFM and LEFM.